ADVANCED FUNCTIONAL MATERIALS
www.afm-journal.de

Hierarchical Composites of Single/Double-Walled Carbon Nanotubes Interlinked Flakes from Direct Carbon Deposition on Layered Double Hydroxides

By *Meng-Qiang Zhao, Qiang Zhang, Xi-Lai Jia, Jia-Qi Huang, Ying-Hao Zhang,* and *Fei Wei**

Three-dimensional hierarchical nanocomposites consisting of one-dimensional carbon nanotubes (CNTs) and two-dimensional lamellar flakes (such as clay, layered double hydroxides) show unexpected properties for unique applications. To achieve a well-designed structure with a specific function, the uniform distribution of CNTs into the used matrix is a key issue. Here, it is shown that a hierarchical composite of single/double-walled CNTs interlinked with two-dimensional flakes can be constructed via in-situ CNT growth onto layered double hydroxide (LDH) flakes. Both the wall number and diameter of the CNTs and the composition of the flakes can be easily tuned by changing the proportion of the transition metal in the LDH flakes. Furthermore, a structure with continuously interlinked CNT layers alternating with lamellar flakes is obtained after compression. The hierarchical composite is demonstrated to be an excellent filler for strong polyimide films. This study indicates that LDH is an extraordinary catalyst for the fabrication of hierarchical composites with high-quality single/double-walled CNTs. The as-obtained CNTs/calcined LDHs nanocomposite is a novel structural platform for the design of mechanically robust materials, catalysts, ion-transportation, energy-conversion, and other applications.

1. Introduction

Combining materials with 1D nanowires/nanotubes and 2D lamellar flakes leads to 3D hierarchical nanocomposites with unexpected properties for unique applications.[1–6] For instance, the combined 3D clay–polymer composites and clay–carbon nanotube (CNT) nanocomposites show extraordinary mechanical and energy-absorbing properties.[2–6] The key issue for the successful application of nanocomposites lies in the ability to manipulate the arrangement of the two phases (filler and matrix) into a well-designed structure.[3,5,7] For example, when the CNTs (filler) are well dispersed as an enhanced network into a polymer (matrix), the mechanical, electrical, and energy-absorbing properties can be significantly improved.[4,5,8–10] Good dispersion of CNTs in the matrix or other solvents is believed to be a key issue to obtain nanocomposites with extraordinary performance. Thus, surfactants, biomacromolecules, copolymers, DNA, and clays have widely been used for CNT dispersion through shearing or sonication processes.[11] Ionic liquids have also been selected as a solvent to achieve good dispersion of CNTs.[12] However, those procedures are usually complicated. Furthermore, the CNTs might be flocculated into CNT bundles or CNT agglomerates because of strong van der Waals interactions during the further mixing and casting procedures. Up to now, the uniform distribution of CNTs into certain matrices with a well-designed structure and certain function has been a challenge.

Recently, it has been shown that CNTs can be directly synthesized on various kinds of matrices to controllably fabricate nanocomposites. Cao et al. grew CNTs on a SiC fiber and the obtained multifunctional brush could be used for several unique tasks such as cleaning nanoparticles from narrow spaces, coating the internal spaces of holes, and functioning as movable electromechanical brush contacts and switches.[13] Woven SiC fiber/CNT composites via in-situ growth showed remarkable improvements in the interlaminar fracture toughness, hardness, delamination resistance, damping, and electrical conductivities.[6] CNT(Ni)/Al composites with homogeneously dispersed CNTs within the Al powders have been obtained by the in-situ growth of CNTs on an Al matrix with low Ni content.[14] The hardness and tensile strength of the CNT(Ni)/Al matrix composites were 2.0 and 1.8 times higher than those of the same composites obtained by dispersion/mixing methods.[14] Zhang et al. directly grew CNTs on clays and found that the as-obtained products could be directly filled into a nylon-6 matrix to significantly improve its tensile strength.[15] These results all indicate that the in-situ synthesis of

[*] Prof. F. Wei, Dr. M. Q. Zhao, Dr. Q. Zhang, X. L. Jia, J. Q. Huang, Y. H. Zhang
Beijing Key Laboratory of Green Chemical Reaction Engineering and Technology
Department of Chemical Engineering
Tsinghua University
Beijing 100084 (P.R. China)
E-mail: wf-dce@tsinghua.edu.cn

DOI: 10.1002/adfm.200901522

CNTs on certain matrices achieved very good dispersion[13–16] and the as-obtained composites generally showed excellent performances. Compared to traditional procedures, in-situ nanocomposite fabrication strategies are quite easy to achieve and cost less. However, in these studies only multiwalled CNTs (MWCNTs) were used for the in-situ fabrication of nanocomposites on certain matrices.[6,13–16] It should be noted that single/double walled CNTs (S/DWCNTs) have a much more ideal structure in terms of their smaller diameter, larger aspect ratio, and lower defect density.[17–20] Compared to MWCNTs, S/DWCNTs exhibit better mechanical, thermal, and electrical properties, and can be found in a wide range of applications, such as, in high-performance nanocomposites, high electron mobility components for electronics, and field-emission displays.[21] If 1D S/DWCNTs can be controllably synthesized on 2D flakes to fabricate a hierarchical composite, novel advanced functional materials with well-dispersed S/DWCNTs could be obtained.

However, the direct growth of S/DWCNTs on the matrices mentioned above (such as SiC fibers, carbon fibers, Al metal, or clays) is not so easy. The reason lies in the difficulty of obtaining a uniform distribution of small catalyst particles (0.5–5 nm) on those matrices at high temperature (750–1300 °C).[18,22] MgO, Al_2O_3, and SiO_2 have previously been studied as supports for the growth of S/DWCNTs,[19,20] however, they were found to cause random nanoparticle agglomeration when being used as catalyst supports for S/DWCNT growth.[19,20,22] Thus, they cannot be used as the 2D material to promote the dispersion of S/DWCNTs. Recently, layered double hydroxides (LDHs), also known as hydrotalcite-like materials, which are a class of 2D nanostructured anionic clays whose structure is based on brucite ($Mg(OH)_2$)-like layers, can be easily and controllably synthesized on a large scale.[23,24] Most metals, such as Fe, Co, Ni, Cu, Zn, Mg, Al, Ca, and Li, can be arranged on the atomic level in a lamellar LDH flake with controllable components. This is attributed to the substitution of divalent metal cations by trivalent cations within their hydrotalcite-like layers, which leads the LDH layer to be positively charged and balanced by a wide variety of anions within their interlayer domains. Compared to natural clay, the composition of LDHs is much simpler and can be anticipated, which is very important for their use in actual catalysts, catalyst precursors, or catalyst supports.[24] After calcination and reduction metal particles can be produced that are uniformly distributed on the flakes and that function as good catalysts for CNT growth. A few reports have described the in-situ growth of CNTs on LDHs.[25] However, only random MWCNTs with a diameter ranging from 10 to 50 nm and a specified surface area of less than 50 $m^2\ g^{-1}$ were synthesized in most cases.[25] Compared to MWCNT growth, high temperatures and small catalyst particles are needed for S/DWCNT growth. Thus the composition of the LDH flakes and the growth window need to be explored carefully. Moreover, the morphology of the LDHs after growth has rarely been mentioned and the performance of the composites of CNTs and calcined LDH (c-LDH) flakes has seldomly been investigated.

For this report, we used Fe/Mg/Al LDHs, as well as Co/Mg/Al, Ni/Mg/Al, and Co/Fe/Mg/Al LDHs as the catalyst precursor, and we explored the idea of the in-situ fabrication of S/DWCNTs interlinked with lamellar flakes that directly formed a 3D hierarchical nanocomposite. As shown in Scheme 1, the LDHs were used as the 2D lamellar flakes for CNT growth. After calcination and reduction, metal particles with small sizes could be produced. By introducing a carbon source a well-controlled CNT interlinked hierarchical nanocomposite was obtained. After characterization by Raman spectroscopy and transmission electron microscopy (TEM), we found that the CNTs mainly consisted of S/DWCNTs. Moreover, the hierarchical composites could be further pressed into a continuous CNT layer alternating with lamellar c-LDH flakes to form a layered structure. A high-performance CNTs/c-LDHs/polyimide (PI) film was fabricated from the as-grown products to show the extraordinary performance of the hierarchical composite of S/DWCNTs interlinked with c-LDH flakes.

2. Results and Discussion

2.1. Hierarchical Composites of CNTs Interlinked with c-LDH Flakes

A series of Fe/Mg/Al LDH flakes with different iron content were prepared using a co-precipitation reaction, and named as LDH A–E as shown in Table 1. As illustrated in Figure 1a, the as-obtained LDH-C samples show the typical morphology of LDH flakes. One can see clearly that the LDHs are plate-like hexagonal particles with lateral sizes ranging from 1 to 2 μm. A typical powder X-ray diffraction (XRD) pattern for the as-synthesized LDH-C is shown in Figure 1b. The sharp and symmetric features of the diffraction peaks strongly suggest that the produced Fe/Mg/Al LDH flakes were highly crystallized, possessing a 3D order. In addition, all the diffraction peaks could be indexed as a rhombohedral structure with the refined lattice parameters of $a = 0.2994$ nm and $c = 2.2125$ nm. The chemical composition of the prepared LDH A–E samples obtained by elemental analysis is shown in Table 1.

The hierarchical composites A–E were obtained after direct growth of CNTs on LDH A–E by a facile chemical vapor deposition (CVD) process (Table 1). Typical scanning electron microscopy

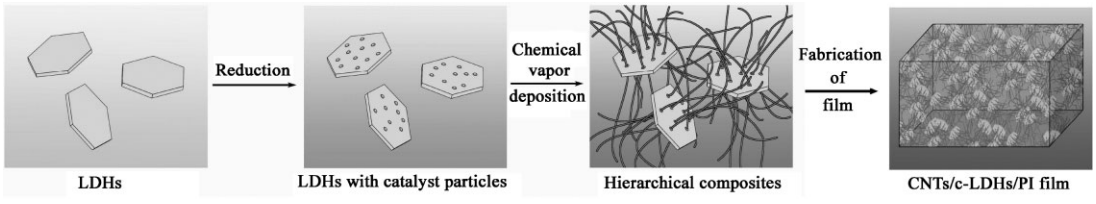

Scheme 1. Schematic illustration showing the procedure for constructing hierarchical composites of single/double-walled carbon nanotubes interlinked LDHs and the incorporation of CNT/c-LDHs hybrid fillers into a PI matrix to make a CNTs/c-LDHs/PI film.

Table 1. The properties of hierarchical composites of S/DWCNTs interlinked flakes obtained from direct carbon deposition on Fe/Mg/Al layered double hydroxides.

Samples	LDHs	Composition of as-prepared LDHs (n(Fe)/n(Mg)/n(Al))	SSA_{CNTs} [m^2 g^{-1}]	CNTs content	I_D/I_G
Composite-A	LDH-A	0.05: 1.85: 1	1289.0	15%	0.06
Composite-B	LDH-B	0.10: 1.53: 1	1017.1	30%	0.04
Composite-C	LDH-C	0.20: 1.99: 1	941.6	36%	0.03
Composite-D	LDH-D	0.36: 1.87: 1	770.9	32%	0.04
Composite-E	LDH-E	0.83: 1.61: 1	498.1	25%	0.11

(SEM) images of the composites B and C are shown in Figure 2a and b, respectively. It can be observed that the use of a short growth duration results in the formation of a large amount of CNTs interlinked in the c-LDHs. Powder XRD analysis showed that the hydrotalcite-like structure of the LDHs was lost after the calcination, leaving metal oxides and spinellites as the major elements (Fig. S1). However, the plate-like hexagonal morphology was well preserved and the size was hardly changed after calcination. The fine CNTs intercrossed among the architecture showed a lamellar structure. The CNT content in the as-grown composite C was 36%, indicating that about 0.56 g of CNTs were grown on 1.0 g of c-LDH flakes. Figure 2c shows a typical TEM image of the CNTs in composite C. High-resolution TEM (HRTEM) (Fig. 2d) indicated that the CNTs, which are interlinked among the lamellar particles, mainly consisted of S/DWCNTs.

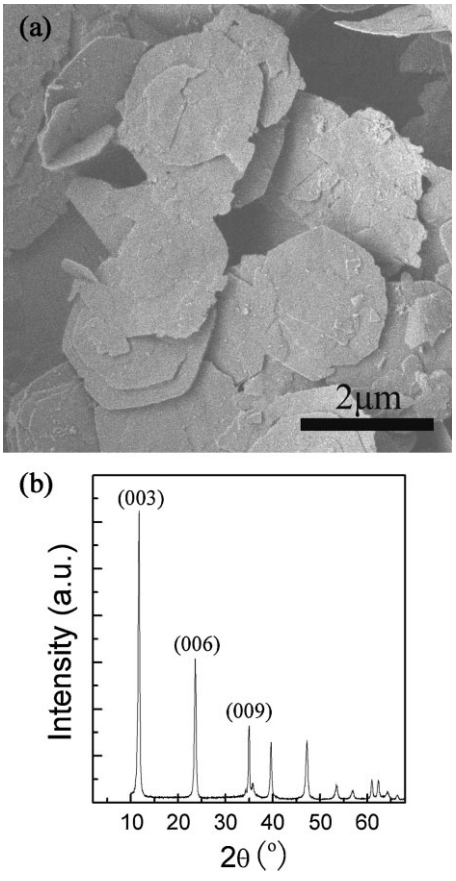

Figure 1. a) SEM image and b) XRD pattern of LDH-C.

They have a small and uniform diameter ranging from 1.5 to 5.0 nm, which is to be discussed further in detail in the following section. Moreover, it can be seen from both the SEM and TEM images that the obtained S/DWCNTs are not strongly entangled. This may be attributed to the orientating function of the c-LDH flakes. It is clear that the roots of the synthesized CNTs are fixed at certain spots of the c-LDH flakes thus preventing aggregation. In this way hierarchical nanocomposites composed of S/DWCNTs interlinked flakes were obtained. The flakes were individually distributed among the entangled S/DWCNTs. This led to a hierarchical structure with the advantage of being able to change the morphology of an ordered material with a layered structure consisting of interlinked S/DWCNT layers alternating with lamellar particles. Moreover, the existence of flakes effectively promoted the homogeneous dispersion of the S/DWCNTs.

A few other reports have described the growth of MWCNTs on Co/Al, Co/Fe/Al, Ni/Mg/Al, and Fe/Zn/Al LDHs.[25] There were also some reports on carbon nanofibers or MWCNTs grown on natural clay[15,26] or lava.[27] However, very few S/DWCNTs were synthesized in these reports. Here, the production of uniform, hierarchical composites of S/DWCNTs interlinked with flakes was

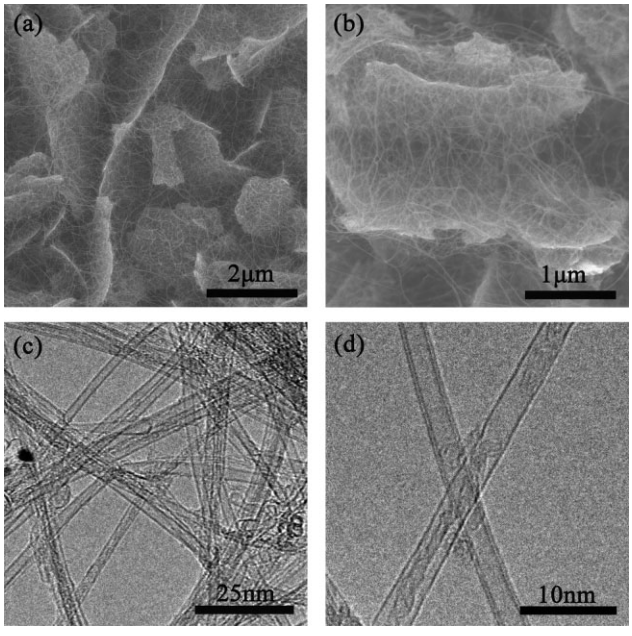

Figure 2. SEM and TEM images of the obtained hierarchical composites from CH_4 over Fe/Mg/Al LDHs at 900 °C. a) SEM image of composite B; b) SEM image of composite C; c) TEM image of CNTs in composite C; d) HRTEM image of CNTs in composite C.

realized by an in-situ growth via a facile CVD process. A family of LDH flakes, such as Fe/Mg/Al, Co/Mg/Al, Ni/Mg/Al, and Co/Fe/Mg/Al LDH flakes, was selected as catalyst precursor to synthesize the S/DWCNTs. The metal content (Fe, Co, and/or Ni) in the LDHs ranged from 0.2 to 15%. Furthermore, high temperatures (900 °C) were used to form small catalyst particles (0.5–5 nm) for SWCNT and/or DWCNT growth without the need for a H_2 reduction step. Both the catalyst composition and the growth parameter selection were important for the S/DWCNT growth. All LDH flakes (Co/Mg/Al, Ni/Mg/Al, and Co/Fe/Mg/Al) were demonstrated to be effective catalysts for the construction of hierarchical composites as is shown in the Supporting information (Figs. S2–S4). For example, with Fe/Mg/Al LDHs serving as the catalyst, about 40% of single-walled and 60% of double-walled CNTs were obtained when the Fe content was 3.0 wt % and a mean surface area of 942 $m^2\ g^{-1}$ was found. The intensity ratio of the Raman D-band over the G-band (I_D/I_G) was just 0.03, which was obviously lower than that of CNTs grown on Fe/Mg/O,[28] Fe/Mo/Mg/O,[17] or Fe/Mo/Al/O[20] catalysts. These indicated that the as grown CNTs were of a high quality containing few defects. A novel general strategy using LDH flakes serving as a catalyst for the growth of high-quality S/DWCNTs was thus realized.

2.2. Tuning of the Diameter and Wall Number Distribution of CNTs in the Hierarchical Nanocomposites

Apart from the interesting structures obtained above, it should be noted that not only the composition of the c-LDHs, but also the structure of the CNTs in the hierarchical composites can be adjusted. Here we discuss the facile strategy to modulate the wall number, diameter, and content of the CNTs in the hierarchical composites by simply changing the iron proportion in the LDH flakes.

A series of Fe/Mg/Al LDH with different Fe content were used for S/DWCNT growth (Table 1), and similar hierarchical composites were obtained, see before. The TEM and HRTEM images for the CNTs in composites A, C, and E are presented in Figure 3a to f. The distributions of the wall number and the outer

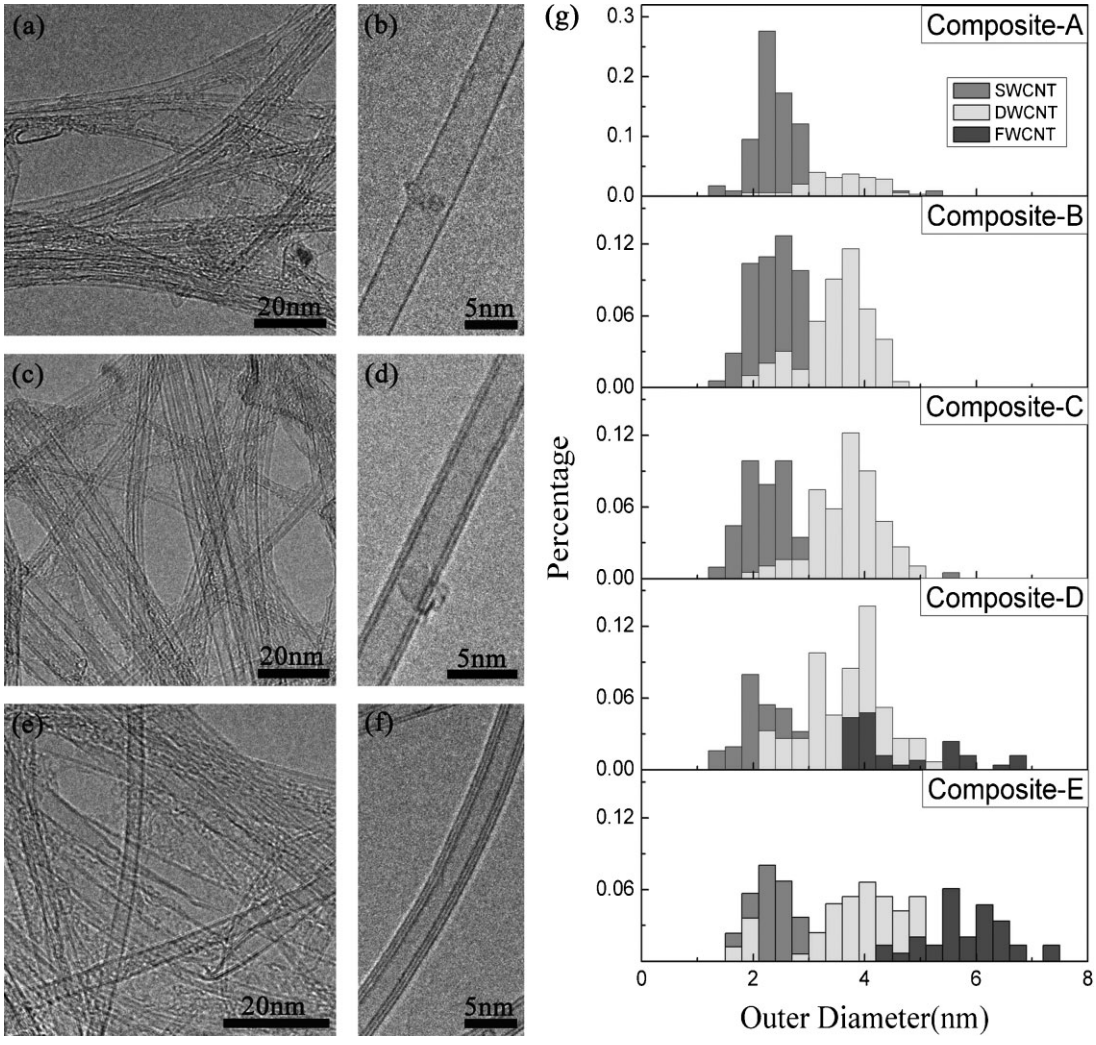

Figure 3. TEM and HRTEM images of CNTs in a,b) composite A; c,d) composite C; e,f) composite E. g) Distribution of the outer diameter for obtained S/D/FWCNTs in composites A–E.

diameter of the CNTs were obtained by measuring around 200 individual CNTs in the HRTEM images, as shown in Figure 3g. For composite A, only SWCNTs and DWCNTs were found, and the amount of SWCNTs could be up to about 77% according to the statistical results. The specific surface area (SSA) of CNTs in composite A was around 1289.0 $m^2 g^{-1}$ (Table 1). This is close to the theoretical value of individual SWCNTs (1315 $m^2 g^{-1}$), and it is higher than that of DWCNTs (700–850 $m^2 g^{-1}$), MWCNTs (200–600 $m^2 g^{-1}$), and SWCNT bundles (100–700 $m^2 g^{-1}$).[29] This indicates that Fe/Mg/Al LDH flakes with a low iron content show a good selectivity for SWCNT growth, whereby the SWCNTs were also well dispersed. The CNT content in composite A was about 15%. With increasing iron content, more DWCNTs and MWCNTs were found (composites B–E (Fig. 3g)), while the SSA of the CNTs showed an obvious decreasing trend (Table 1). The CNT contents in composites B and C increased to 30% and 36%, indicating that more carbon was deposited on the catalysts. However, the SSA of the CNTs decreased to 1017.1 $m^2 g^{-1}$ and 941.6 $m^2 g^{-1}$, respectively. The statistical proportion of SWCNTs in composites B and C is shown to be 52% and 43%, respectively (Fig. 3g). With further increasing Fe content in the LDH flakes, the SSA of the CNTs further decreased (Table 1), and more and more MWCNTs were found in the as-grown products (Fig. 3g). It should be noted that the wall numbers of these observed MWCNTs were not higher than 5, the reason for which we call them few-walled CNTs (FWCNTs).[30] For composite D, the proportions of DWCNTs and FWCNTs were shown to be 56% and 17%, respectively, whereas those for composite E were statistically calculated to be 43% and 24%, respectively. The CNT content in composites C and D decreased a little (Table 1), which can be attributed to a catalyst deactivation caused by the formation of catalyst particles with larger sizes. An obvious characteristic of the outer-diameter distributions of the CNTs can be seen in Figure 3g. The outer diameter of the CNTs has a distinct dividing line for all samples. The distribution of the outer diameter of the SWCNTs was mainly concentrated on 1.5 to 3.0 nm, while for DWCNTs, it mostly ranged from 3.0 to 5.0 nm. For FWCNTs, outer diameters above 5.0 nm were commonly seen.

The diameter of the CNTs depended heavily on the diameter distribution of the catalyst particles at the growth temperature.[31] In the LDH flakes, the iron ion is inserted into the hydrotalcite-like layers by isomorphous substitution of Mg^{2+}.[23] Thus, they are distributed uniformly in the layers at an atomic level. After calcination and reduction, the Fe^{3+} will be reduced into Fe nanoparticles. As shown in Figure 4a, there are large amount of catalyst particles with a size smaller than 5 nm distributed on the flakes. During the CVD process, the carbon source will decompose at the surface of these nanoparticles and the dominating surface diffusion of the carbon atoms on the catalyst particles results in the formation of SWCNTs.[32] With increasing size of the catalyst particles, both surface and bulk diffusion, which correspond to the formation of the outer and inner layer of DWCNTs, respectively, take place on a single catalyst particle.[33] Thus, SWCNTs are more inclined to form (Fig. 4b) on particles that are smaller than 3 nm, and DWCNTs usually grow on particles in the size range of 3–5 nm (Fig. 4c). While for particles larger than 5 nm, the formation of FWCNTs and carbon-sphere-encapsulated particles lead to catalyst deactivation (Fig. 4d). The results in Figure 3g can therefore easily be explained by the fact that with increasing iron content the catalyst particles grow larger during the reduction course.

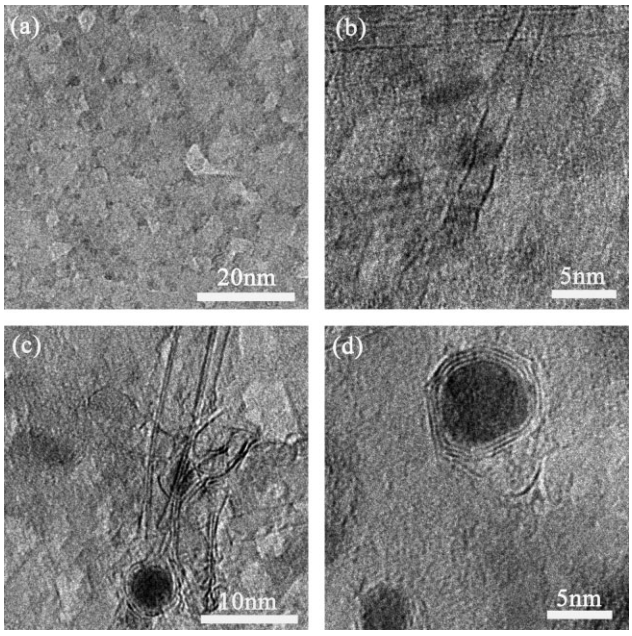

Figure 4. a) Catalyst particles on LDH-C after calcination and reduction. b) SWCNT grown from a catalyst particle smaller than 3 nm on LDH-A. c) DWCNT grown from a catalyst particle with a size of 4 nm on LDH-C. d) Carbon spheres encapsulated catalyst particles with a size of 7 nm on LDH-E.

2.3. Compressing of CNTs Interlinked in Hierarchical Composites into Alternating CNTs/c-LDHs

We have found that the constitution of the hierarchical composites can be easily modulated by changing the composition of the LDHs. Furthermore, from the SEM images demonstrated in Figure 2, the CNTs are in a low-density, well-dispersed state, and the CNTs interlinked with c-LDH flakes show abundant pores. As shown in Figure 5, the synthesized CNTs occupy the interspaces between the lamellar c-LDH particles, leading to the reduction of the pore volume of pores between 230 and 3000 nm in diameter. However, the volume of pores ranging from 5 to 230 nm increased significantly, indicating that CNTs have a certain possibility to broaden the pores among c-LDH flakes and thus promote the dispersion of c-LDH flakes. Because of the good electrical conductivity and abundant mesopores and macropores, hierarchical composites of S/DWCNTs interlinked flakes can potentially be used for applications in supercapacitors and Li-ion batteries.[34] Furthermore, the hierarchical composites can easily be densified by simple compression. As shown in Figure 6, when the as-prepared hierarchical composite is compressed in a die at a pressure of 100 MPa, a block of densified CNTs/c-LDHs can be obtained. The compressed block shows a uniform pore-size distribution ranging from 5 to 12 nm (Fig. 6b), which can be attributed to the interspaces between lamellar particles or between the CNTs. The density of the block was measured to be 1.8 $cm^3 g^{-1}$,

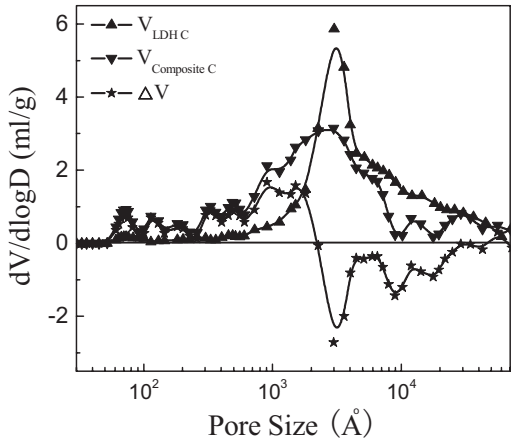

Figure 5. Pore-size distributions for prepared LDH-C and the obtained hierarchical sample of composite C.

which is 85 times higher than that before the compression. The volume fraction of the CNTs in the block is estimated to be around 60%. The schematic illustration for the structure of the block is shown in the inserted picture. It can be seen from the SEM image of the cross section of the block cleaved with a razor that the block shows a clearly layered structure, as shown in Figure 6c. Aligned S/DWCNTs with high density were formed following the line of cleaving on the cross section of the block because of the pliability, toughness, and easy-combing properties of the CNTs interlinked with c-LDH flakes. From the bird's-eye view of the compressed block, as shown in Figure 6d, it can be seen that the

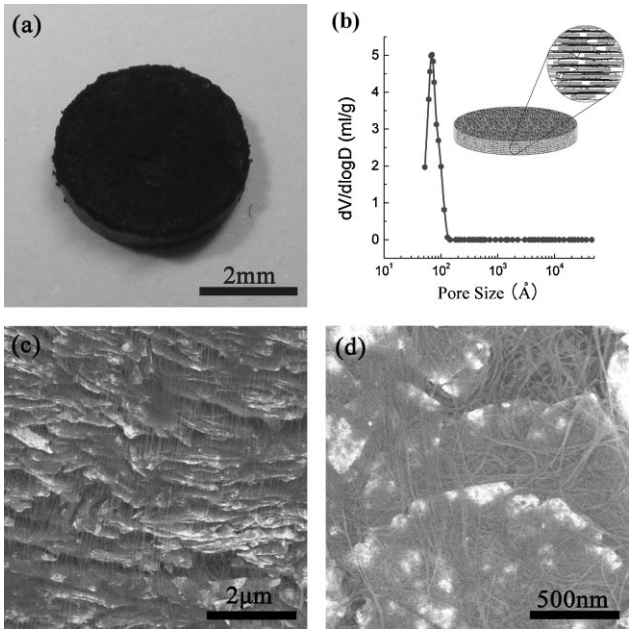

Figure 6. a) A block of the CNTs/c-LDHs nanocomposites after compression at a pressure of 100 MPa. b) Pore-size distribution of the compressed composite C, the inset shows a schematic illustration of the structure of the block. c) SEM image of the cross section and d) a bird's eye view of the block.

layered structure consists of interlinked CNT layers alternating with lamellar c-LDH particles. Thus a great ordered material with layered structure composed of interlinked S/DWCNT layers alternating with lamellar particles was obtained after the hierarchical composite was compressed at high pressure. Thousands of layers of CNTs and c-LDH flakes were assembled into an alternating structure that will have great potential in high-performance composites, energy storage and -conversion, sensors, and other applications.[3,35]

2.4. Fabrication of Strong CNTs/c-LDHs/PI Films

The CNTs/c-LDHs hierarchical composite discussed above is expected to be an ideal filler for high-performance polymers because of the homogenous dispersion of both CNTs and LDH flakes. In order to demonstrate the enhancement effect of the prepared filler, we have fabricated CNTs/c-LDHs/polyimide (PI) films via an in-situ polymerization method using composite C. The reasons for using PI for this is that PI is a polymer with good transparency, toughness, and light weight, and it is under consideration for applications in advanced spacecraft, in indium tin oxide (ITO) soleplates for liquid crystal displays, in solar cell soleplates, and in optical waveguides for communication purposes.[36] Increasing the mechanical properties of PI is an important issue to realize those applications. Here, the as-obtained stress–strain curves are shown in Figure 7a, and the tensile properties of neat PI and CNTs/c-LDHs/PI film are summarized in Table 2. It can be seen that the incorporation of only 0.40 wt % of composite C significantly improves the mechanical properties of PI. The elastic modulus of PI is improved from 651.3 to 770.9 MPa, and the tensile strength is improved from 78.1 to 109.1 MPa. The elongation-at-break of the composite film increases significantly from 26.6% to 59.6%, indicating that PI becomes more robust after the incorporation of the CNTs/c-LDHs hybrid filler. The energy absorbed[10] during the tensile testing is improved by 220% (Table 2). These results indicate that the mechanical properties of the CNTs/c-LDHs/PI film are substantially superior to those of neat PI.

It is very interesting to compare the mechanical properties of the CNTs/c-LDHs/PI film with those of CNTs/PI films with various loading levels of purified CNT filler. Yu et al. reported that the incorporation of 0.30 wt % SWCNTs into PI leads to an increase of the tensile strength by only 5% and an increase of the Young's modulus by 18%.[9] Zhang et al. prepared composites containing functionalized CNTs and PI, and the measurement of the mechanical properties showed that the addition of 1.0 wt % MWCNTs in the PI matrix caused a small increase of 6.7% in the tensile strength and an increase of 29.8% in the Young's modulus.[37] Here, the elastic modulus of PI is improved by about 20%, and the tensile strength is improved by about 40%. The enhancement of the mechanical properties upon incorporation of 0.40 wt % CNTs/c-LDHs filler is thus even higher than that in the case of using neat CNTs alone. The high performance of the composite is obviously related to the homogeneous dispersion of both the 1D CNTs and the 2D c-LDH flakes. Figure 7b shows a high-resolution SEM image of the fractured surface of a CNTs/c-LDHs/PI film after tensile testing. It clearly

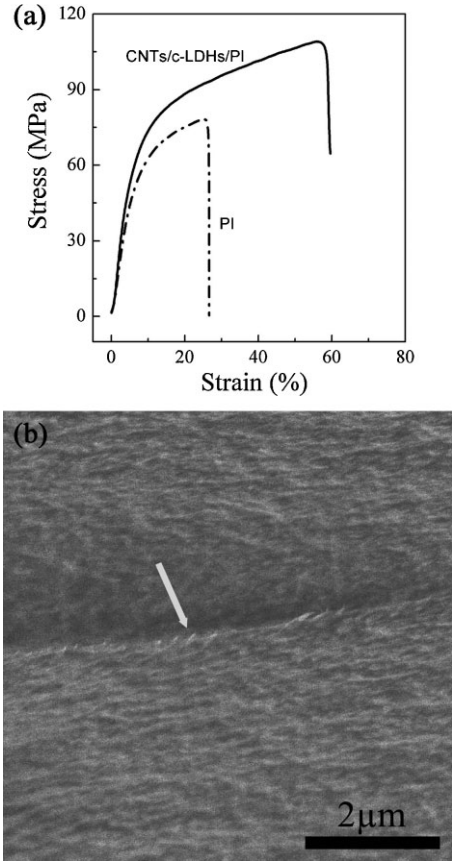

Figure 7. a) Stress–strain curves of a neat PI and a composite CNTs/c-LDHs/PI film containing 0.40 wt % CNTs/c-LDHs hybrid filler. b) SEM image of the typical morphology of the failure surface of a CNTs/c-LDHs/PI film.

shows that the CNTs/c-LDHs hierarchical composite has a close interfacial connection with the PI matrix, which is indicated by the white arrow. The jagged line is the c-LDH flake and the small bright dots are the ends of the ruptured CNTs on the fractured surface. The observation that most CNTs were broken upon failure rather than just pulled out of the matrix is clear evidence of the strong interfacial adhesion between the CNTs/c-LDHs filler and the PI matrix. This is responsible for the significant reinforcement of the mechanical properties of the prepared film. Moreover, because of the uniform distribution of S/DWCNTs in the c-LDHs, the composite can also be used for the self-organization of ordered structures to improve the electrical and thermal conductivities of various polymers. The CNTs/c-LDHs composite is a good platform for wide applications of CNTs in catalysis, ion-transportation, and energy-conversion areas.

3. Conclusions

Hierarchical composites of S/DWCNTs interlinked with flakes were constructed via direct carbon deposition on LDH flakes. The lamellar structure of the LDHs was preserved; moreover, they were individually distributed among the entangled S/DWCNTs. The synthesized CNTs showed large SSA values, little defects, and were obtained in high yield. The combination of the 1D CNTs and the 2D c-LDH flakes promoted CNT dispersion. The diameter and wall number of the CNTs could easily be tuned by changing the proportion of iron in the LDHs. A lower iron content favored the growth of SWCNTs because of the formation of large amounts of catalyst particles smaller than 3 nm. While for higher iron content, catalyst particles with a size ranging from 3 to 5 nm were more likely to be formed and the growth of DWCNTs was favored. A structure composed of interlinked CNT layers alternating with lamellar flakes could be obtained after the compression of the hierarchical composites. The mechanical properties of CNTs/c-LDHs/PI films were demonstrated to have been significantly improved compared to neat PI. This work provides a novel structural platform towards the design of mechanically robust materials; it also provides novel materials for catalytical, ion-transportation, energy-conversion, and other applications.

4. Experimental

Preparation of LDH Flakes: The Fe/Mg/Al LDH flakes were prepared using a co-precipitation reaction. $Mg(NO_3)_2 \cdot 6H_2O$, $Al(NO_3)_3 \cdot 9H_2O$, and urea were dissolved in 250.0 mL of deionized water with $[Mg^{2+}] + [Al^{3+}] = 0.15$ mol L^{-1}, $n(Mg)/n(Al) = 2{:}1$, $[urea] = 3.0$ mol L^{-1}. $Fe(NO_3)_3 \cdot 9H_2O$ was then dissolved in the solution, the molar ratios of Fe to Al were controlled at 0.05, 0.1, 0.2, 0.4, and 0.8, respectively. The prepared solution was heated to 100 °C under continuous magnetic stirring for 12 h in a flask (equipped with a reflux condenser) of 500.0 mL under ambient atmosphere. Then, the obtained suspension was kept at 95 °C for another 12 h without stirring. After filtering, washing, and freeze-drying, the final products were ground to brown–yellow powders with different color depths. The LDH flakes obtained were named as LDH A–E. The other LDH flakes were prepared through the same process. The composition of these LDH flakes was fixed as $n(Co)/n(Mg)/n(Al) = 0.4{:}2{:}1$, $n(Ni)/n(Mg)/n(Al) = 0.4{:}2{:}1$ and $n(Co)/n(Fe)/n(Mg)/n(Al) = 0.2{:}0.2{:}2{:}1$.

Construction of Hierarchical Composites of CNTs Interlinked Lamellar Flakes: The preparation of hierarchical composites of CNTs interlinked lamellar flakes was carried out using a catalytic chemical vapor deposition (CVD) process. About 10 mg of the LDH catalyst was sprayed uniformly into a quartz boat, which was then placed at the center of a horizontal quartz tube inserted into a furnace at atmospheric pressure. Then the furnace was heated under flowing Ar (600 mL min^{-1}). On reaching 900 °C, the flow rate of Ar was turned down to 100 mL min^{-1} and maintained as such for 10 min. CH_4 (500 mL min^{-1}) was then introduced into the reactor for 5 min after which H_2 (50 mL min^{-1}) was also added. The growth was maintained for 30 min at 900 °C before the furnace was cooled to room temperature under Ar flow. The as-obtained powders were named as composite A to E, corresponding to their starting LDH A to E.

Table 2. Tensile properties of neat PI and its composite CNTs/c-LDHs/PI containing 0.40 wt % CNTs/c-LDHs hybrid filler.

Samples	Tensile modulus [MPa]	Tensile strength [MPa]	Elongation-at-break [%]	Energy absorbed [kJ kg^{-1}]
Neat PI film	651.3	78.1	26.6	19.1
CNTs/c-LDHs/PI films	770.9	109.1	59.6	60.9

Fabrication of CNTs/c-LDHs/PI Films: Composite C was used as the reinforcement filler, and the synthesis procedure for a typical well-dispersed CNTs/c-LDHs/PI film was as follows: composite C (0.025 g) and 4,4′-diaminodiphenyl ether (3.006 g, 98%) were first dispersed in dimethyl acetamide (65 mL) in an ultrasonic bath for 3 h at room temperature in N_2 atmosphere to yield a uniform suspension. Then, pyromellitic dianhydride (3.341 g, >98.5%) was dissolved in the suspension under strong stirring in an ice-water bath for 1 h under N_2 protection. The obtained suspension was then put into vacuum for 2 h to get rid of the bubbles existing in the suspension. After that, the suspension was poured onto glass slides, and a film-coating device was used to coat films with a thickness of around 60 μm. These glass slides with coated films were dried at 50 °C for 12 h to remove the solvent. The dried films were then placed at the center of a horizontal quartz tube inserted into a furnace at atmospheric pressure and under Ar protection. The furnace was operated following a fixed temperature program for in-situ polymerization of PI. It was heated from room temperature to 100 °C over a period of 60 min and was then maintained at this temperature for another 60 min. After this, the furnace was further heated to 200 °C over 100 min, and kept there for 60 min. Then the temperature was raised to 300 °C over another 100 min and the furnace was again kept at that temperature for 60 min. Finally, the furnace was cooled down to room temperature under an Ar atmosphere, and the obtained PI/LDH-CNT nanocomposite films were peeled off from the glass slides for tensile testing. The neat PI films were prepared in a similar way without the incorporation of composite C.

Characterization: The samples were characterized using a JSM 7401F (JEOL Ltd., Tokyo, Japan) scanning electron microscope operated at 5.0 kV and a JEM 2010 (JEOL Ltd., Tokyo, Japan) transmission electron microscope operated at 120.0 kV. Energy-dispersive spectroscopy (EDS) analysis was performed using a JSM-7401F apparatus with the analytical software INCA, and the accelerating voltage applied was 15.0 kV. XRD patterns were recorded on a Rigaku D/max-RB diffractometer at 40.0 kV and 120 mA using Cu Kα radiation. Raman spectra were obtained under He–Ne laser excitation at 514 and 633 nm using a Renishaw RM2000 spectrometer. The carbon content was obtained by thermogravimetric analysis under heating at 10 °C min^{-1} using Q500. The pore-size distribution of the samples was measured by an ex-situ Hg penetration method. The BET specific surface area of all samples was measured by N_2 adsorption at liquid-N_2 temperature using a Micromeritics Flow Sorb II 2300. The tensile tests were operated on an electronic universal testing machine WDW 3020 at a stretching rate of 5.0 mm min^{-1}.

Acknowledgements

The authors thank Prof. Dang-Sheng Su from the Fritz Haber Institute of the Max Planck Society, Germany, for instructive discussions. The work was supported by the Natural Scientific Foundation of China (No. 20736004, No. 20736007, No. 2007AA03Z346) and the China National Program (No. 2006CB0N0702). Supporting Information is available online from Wiley InterScience or from the author.

Received: August 13, 2009
Published online: January 19, 2010

[1] a) P. B. Messersmith, E. P. Giannelis, *Chem. Mater.* **1994**, *6*, 1719. b) S. S. Ray, M. Okamoto, *Prog. Polym. Sci.* **2003**, *28*, 1539.
[2] a) E. P. Giannelis, *Adv. Mater.* **1996**, *8*, 29. b) D. F. Schmidt, F. Clement, E. P. Giannelis, *Adv. Funct. Mater.* **2006**, *16*, 417.
[3] a) Q. Zhang, M. Q. Zhao, Y. Liu, A. Y. Cao, W. Z. Qian, Y. F. Lu, F. Wei, *Adv. Mater.* **2009**, *21*, 2876. b) L. Y. Jiang, C. M. Leu, K. H. Wei, *Adv. Mater.* **2002**, *14*, 426.
[4] a) P. Dubois, M. Alexandre, *Adv. Eng. Mater.* **2006**, *8*, 147. b) M. Okamoto, T. Fujigaya, N. Nakashima, *Adv. Funct. Mater.* **2008**, *18*, 1776.
[5] L. Liu, J. C. Grunlan, *Adv. Funct. Mater.* **2007**, *17*, 2343.
[6] V. P. Veedu, A. Y. Cao, X. S. Li, K. G. Ma, C. Soldano, S. Kar, P. M. Ajayan, M. N. Ghasemi-Nejhad, *Nat. Mater.* **2006**, *5*, 457.
[7] Y. J. Xu, G. Weinberg, X. Liu, O. Timpe, R. Schlogl, D. S. Su, *Adv. Funct. Mater.* **2008**, *18*, 3613.
[8] a) E. Frackowiak, K. Metenier, V. Bertagna, F. Beguin, *Appl. Phys. Lett.* **2000**, *77*, 2421. b) E. J. Siochi, D. C. Working, C. Park, P. T. Lillehei, J. H. Rouse, C. C. Topping, A. R. Bhattacharyya, S. Kumar, *Compos. Part B-Eng.* **2004**, *35*, 439. c) J. N. Coleman, U. Khan, W. J. Blau, Y. K. Gun'ko, *Carbon* **2006**, *44*, 1624. d) H. Y. Ma, L. F. Tong, Z. B. Xu, Z. P. Fang, *Adv. Funct. Mater.* **2008**, *18*, 414.
[9] A. P. Yu, H. Hui, E. Bekyarova, M. E. Itkis, J. Gao, B. Zhao, R. C. Haddon, *Compos. Sci. Technol.* **2006**, *66*, 1190.
[10] A. B. Dalton, S. Collins, E. Muñoz, J. M. Razal, V. H. Ebron, J. P. Ferraris, J. N. Coleman, B. G. Kim, R. H. Baughman, *Nature* **2003**, *423*, 703.
[11] a) X. Y. Gong, J. Liu, S. Baskaran, R. D. Voise, J. S. Young, *Chem. Mater.* **2000**, *12*, 1049. b) T. Chatterjee, K. Yurekli, V. G. Hadjiev, R. Krishnamoorti, *Adv. Funct. Mater.* **2005**, *15*, 1832. c) J. Li, P. C. Ma, W. S. Chow, C. K. To, B. Z. Tang, J. K. Kim, *Adv. Funct. Mater.* **2007**, *17*, 3207. d) J. Y. Shin, T. Premkumar, K. E. Geckeler, *Chem. Eur. J.* **2008**, *14*, 6044. e) B. Krause, G. Petzold, S. Pegel, P. Potschke, *Carbon* **2009**, *47*, 602.
[12] J. Y. Wang, H. B. Chu, Y. Li, *ACS Nano* **2008**, *2*, 2540.
[13] A. Y. Cao, V. P. Veedu, X. S. Li, Z. L. Yao, M. N. Ghasemi-Nejhad, P. M. Ajayan, *Nat. Mater.* **2005**, *4*, 540.
[14] C. N. He, N. Q. Zhao, C. S. Shi, X. W. Du, J. J. Li, H. P. Li, Q. R. Cui, *Adv. Mater.* **2007**, *19*, 1128.
[15] W. D. Zhang, I. Y. Phang, T. X. Liu, *Adv. Mater.* **2006**, *18*, 73.
[16] a) N. Yamamoto, A. J. Hart, E. J. Garcia, S. S. Wicks, H. M. Duong, A. H. Slocum, B. L. Wardle, *Carbon* **2009**, *47*, 551. b) J. O. Zhao, L. Liu, Q. G. Guo, J. L. Shi, G. T. Zhai, J. R. Song, Z. J. Liu, *Carbon* **2008**, *46*, 380.
[17] a) A. M. Cassell, J. A. Raymakers, J. Kong, H. J. Dai, *J. Phys. Chem. B* **1999**, *103*, 6484. b) B. C. Liu, S. C. Lyu, S. I. Jung, H. K. Kang, C. W. Yang, J. W. Park, C. Y. Park, C. J. Lee, *Chem. Phys. Lett.* **2004**, *383*, 104. c) Q. Zhang, H. Yu, Y. Liu, W. Z. Qian, Y. Wang, G. H. Luo, F. Wei, *Nano* **2008**, *3*, 45.
[18] P. Nikolaev, M. J. Bronikowski, R. K. Bradley, F. Rohmund, D. T. Colbert, K. A. Smith, R. E. Smalley, *Chem. Phys. Lett.* **1999**, *313*, 91.
[19] a) D. Ciuparu, Y. Chen, S. Lim, G. L. Haller, L. Pfefferle, *J. Phys. Chem. B* **2004**, *108*, 503. b) Y. Li, X. B. Zhang, L. H. Shen, J. H. Luo, X. Y. Tao, F. Liu, G. L. Xu, Y. W. Wang, H. J. Geise, G. Van Tendeloo, *Chem. Phys. Lett.* **2004**, *398*, 276. c) H. Ago, S. Imamura, T. Okazaki, T. Saitoj, M. Yumura, M. Tsuji, *J. Phys. Chem. B* **2005**, *109*, 10. 035.
[20] Q. Zhang, W. Z. Qian, Q. Wen, Y. Liu, D. H. Wang, F. Wei, *Carbon* **2007**, *45*, 1645.
[21] a) R. H. Baughman, A. A. Zakhidov, W. A. de Heer, *Science* **2002**, *297*, 787. b) S. Banerjee, T. Hemraj-Benny, S. S. Wong, *Adv. Mater.* **2005**, *17*, 17.
[22] a) H. M. Cheng, F. Li, G. Su, H. Y. Pan, L. L. He, X. Sun, M. S. Dresselhaus, *Appl. Phys. Lett.* **1998**, *72*, 3282. b) F. Wei, Q. Zhang, W. Z. Qian, H. Yu, Y. Wang, G. H. Luo, G. H. Xu, D. Z. Wang, *Powder Technol.* **2008**, *183*, 10.
[23] D. G. Evans, D. A. Xue, *Chem. Commun.* **2006**, 485.
[24] a) D. P. Debecker, E. M. Gaigneaux, G. Busca, *Chem. Eur. J.* **2009**, *15*, 3920. b) Z. Lue, X. Duan, Chin, J. Catal, **2008**, *29*, 839. c) F. Z. Zhang, X. Xiang, F. Li, X. Duan, *Catal. Surv. Asia* **2008**, *12*, 253.
[25] a) F. Li, Q. Tan, D. G. Evans, X. Duan, *Catal. Lett.* **2005**, *99*, 151. b) Y. Zhao, Q. Z. Jiao, C. H. Li, J. Liang, *Carbon* **2007**, *45*, 2159. c) H. I. Hima, X. Xiang, L. Zhang, F. Li, *J. Mater. Chem.* **2008**, *18*, 1245. d) H. I. Hima, X. Xiang, L. Zhang, F. Li, D. G. Evans, *Chin. J. Inorg. Chem.* **2008**, *24*, 886. e) R. Benito, M. Herrero, F. M. Labajos, V. Rives, C. Royo, N. Latorre, A. Monzon, *Chem. Eng. J.* **2009**, *149*, 455. f) X. Xiang, L. Zhang, H. I. Hima, F. Li, D. G. Evans, *Appl. Clay Sci.* **2009**, *42*, 405.
[26] a) A. Garcia, M. H. Bocanegra-Bernal, C. Dominguez, A. Aguilar-Elguezabal, *Appl. Clay Sci.* **2009**, *45*, 95. b) H. P. Li, N. Q. Zhao, Y. Liu, C. Y. Liang, C. S. Shi, X. W. Du, J. J. Li, *Compos. Part A-Appl. Sci. Manuf.* **2008**, *39*, 1128. c) A. Rinaldi, J. Zhang, J. Mizera, F. Girgsdies, N. Wang, S. B. A. Hamid, R. Schlogl, D. S. Su, *Chem. Commun.* **2008**, 6528.

d) D. Gournis, M. A. Karakassides, T. Bakas, N. Boukos, D. Petridis, *Carbon* **2002**, *40*, 2641. e) A. Bakandritsos, A. Simopoulos, D. Petridis, *Chem. Mater.* **2005**, *17*, 3468. f) Q. Zhang, M. Q. Zhao, J. Q. Huang, Y. Liu, Y. Wang, W. Z. Qian, F. Wei, *Carbon* **2009**, *47*, 2600. g) F. C. C. Moura, R. M. Lago, *Appl. Catal. B-Environ.* **2009**, *90*, 436.

[27] a) D. S. Su, *ChemSusChem* **2009**, *2*, 1009. b) D. S. Su, X. W. Chen, *Angew. Chem. Int. Ed.* **2007**, *46*, 1823. c) D. S. Su, X. W. Chen, X. Liu, J. J. Delgado, R. Schlogl, A. Gajovic, *Adv. Mater.* **2008**, *20*, 3597.

[28] Y. Liu, W. Z. Qian, Q. Zhang, G. Q. Ning, G. H. Luo, Y. Wang, D. Z. Wang, F. Wei, *Chem. Eng. Technol.* **2009**, *32*, 73.

[29] A. Peigney, C. Laurent, E. Flahaut, R. R. Bacsa, A. Rousset, *Carbon* **2001**, *39*, 507.

[30] a) C. Qian, H. Qi, J. Liu, *J. Phys. Chem. C* **2007**, *111*, 131. b) P. Landois, A. Peigney, C. Laurent, L. Frin, L. Datas, E. Flahaut, *Carbon* **2009**, *47*, 789.

[31] a) Y. M. Li, W. Kim, Y. G. Zhang, M. Rolandi, D. W. Wang, H. J. Dai, *J. Phys. Chem. B* **2001**, *105*, 11424. b) E. F. Kukovitsky, S. G. L'Vov, N. A. Sainov, V. A. Shustov, L. A. Chernozatonskii, *Chem. Phys. Lett.* **2002**, *355*, 497. c) Y. Chen, D. Ciuparu, S. Y. Lim, Y. H. Yang, G. L. Haller, L. Pfefferle, *J. Catal.* **2004**, *225*, 453. d) S. Chakrabarti, H. Kume, L. J. Pan, T. Nagasaka, Y. Nakayama, *J. Phys. Chem. C* **2007**, *111*, 1929. e) T. Inoue, I. Gunjishima, A. Okamoto, *Carbon* **2007**, *45*, 2164. f) Q. F. Liu, W. C. Ren, Z. G. Chen, D. W. Wang, B. L. Liu, B. Yu, F. Li, H. T. Cong, H. M. Cheng, *ACS Nano* **2008**, *2*, 1722.

[32] a) H. Ago, K. Nakamura, N. Uehara, M. Tsuji, *J. Phys. Chem. B* **2004**, *108*, 18908. b) R. Seidel, G. S. Duesberg, E. Unger, A. P. Graham, M. Liebau, F. Kreupl, *J. Phys. Chem. B* **2004**, *108*, 1888. c) J. Y. Raty, F. Gygi, G. Galli, *Phys. Rev. Lett.* **2005**, *95*, 096103.

[33] a) R. T. K. Baker, *Carbon* **1989**, *27*, 315. b) F. Ding, A. Rosen, K. Bolton, *Carbon* **2005**, *43*, 2215. c) S. Hofmann, G. Csanyi, A. C. Ferrari, M. C. Payne, J. Robertson, *Phys. Rev. Lett.* **2005**, *95*, 036101. d) R. F. Wood, S. Pannala, J. C. Wells, A. A. Puretzky, D. B. Geohegan, *Phys. Rev. B* **2007**, 75, 235446.

[34] a) E. Frackowiak, F. Beguin, *Carbon* **2002**, *40*, 1775. b) E. Frackowiak, *Phys. Chem. Chem. Phys.* **2007**, *9*, 1774.

[35] a) P. T. Hammond, *Adv. Mater.* **2004**, *16*, 1271. b) X. Zhang, H. Chen, H. Y. Zhang, *Chem. Commun.* **2007**, 1395.

[36] M. X. Ding, *Prog. Polym. Sci.* **2007**, *32*, 623.

[37] Q. H. Zhang, J. Li, X. Zhao, D. J. Chen, *Polym. Int.* **2009**, *58*, 557.